

Dendrite Suppression by a Polymer Coating: A Coarse-Grained Molecular Study

Xian Kong,* Paul E. Rudnicki, Snehashis Choudhury, Zhenan Bao, and Jian Qin*

A major hurdle to the successful deployment of high-energy-density lithium metal based batteries is dendrite growth during battery cycling, which raises safety and cycle life concerns. Coating the Li metal anode with a soft polymer layer has been previously shown to be effective in suppressing dendrite growth, leading to uniform lithium deposition even at high current densities. A 3D coarse-grained molecular model to study the mechanism of dendrite suppression is presented. It is found that the most effective coatings delay or even prevent dendrites from penetrating the polymer layer during deposition. The optimal deposition can be achieved by jointly tuning the polymer stiffness and relaxation time. Higher polymer dielectric permittivity and coating thickness are also effective, but the deposition rate and, therefore, the charging current density is reduced. These findings provide the basis for rational design of soft polymer coatings for stable lithium deposition.

1. Introduction

The proliferation of electric vehicles and personal devices is expected to continue rapidly in coming years, requiring large quantities of low-cost rechargeable batteries with high capacity and energy density.^[1] Commercialized lithium-ion batteries are limited in their theoretical energy density and are not expected to meet electric vehicle pack goals.^[2] Research into new chemistries based on advanced materials is therefore necessary for the development of next-generation batteries.^[3] Lithium metal has many desirable properties as an anode material, including the lowest electrochemical potential (−3.04 V vs the standard hydrogen electrode) and the highest theoretical specific capacity (3860 mAh g^{−1}) among all the candidate materials.^[4] To date, the commercialization of lithium metal anodes in rechargeable batteries has not been successful due to stability and safety issues.^[3] During charging cycles, lithium ions are deposited nonuniformly, which can lead to the growth of dendrites across the cell. This causes significant coulombic efficiency loss, as highly reactive Li metal irreversibly degrades the electrolyte to form unwanted products, decreasing battery capacity. There are also significant safety concerns, as dendritic contact with the


cathode can create a short circuit, causing fires or even explosions. Minimizing or eliminating dendritic growth under commercially viable battery usage conditions has therefore emerged as an important scientific goal in recent decades.^[1]

A wide range of strategies have been attempted to inhibit dendritic growth on lithium metal anodes.^[4] Many approaches are directed at modifying the solid electrolyte interphase (SEI), which spontaneously forms due to the reduction of electrolyte compounds at the Li surface. Creation of a homogeneous, flexible, and mechanically strong SEI has been pursued through the use of a chemically deposited or physically coated artificial SEI on the anode.^[5–8] Driven by theoretical predictions,^[9,10] the use of solid electrolytes to mechanically inhibit dendrite growth has also been

explored. For example, ceramic electrolytes have high ionic conductivity and modulus, but are brittle and show poor adhesion with the Li interface upon cycling.^[11] On the other hand, solid polymer electrolytes (SPEs) are mechanically strong and more adhesive, but suffer from low ionic conductivity, especially at room temperature.^[12,13] Recent approaches in this area have explored self-assembled microstructured block copolymers and layered polymeric and ceramic materials, both aimed at achieving a balance between the necessary properties.^[14–16]

Polymeric electrolytes have many desirable properties for Li battery applications, including enhanced adhesive and elastic properties and relative flexibility in chemical and mechanical properties based on the degree of cross-linking and alterations in functionalization.^[17–19] Polymeric materials are also relatively cost-effective and are easily processed in solution. While they do not have shear moduli on the order of 1–10 GPa, as is required by previous theoretical predictions,^[10] they have nevertheless shown promise in dendrite suppression.^[20–22] For example, polymeric separators strengthened by nanoparticle fillers and polymeric membranes formed through dense crosslinking with hairy nanoparticles have shown the ability to suppress dendrites.^[23,24] Use of a nonporous elastomeric rubber separator improved cycling stability even at high current density (10 mA cm^{−2}).^[19] A novel self-healing polymer (SHP) coating facilitated smooth Li deposition at high current density and enhanced the cycle stability.^[25] More recent continuum theory has partially explained these results by accounting for the separator elasticity in a linear stability analysis.^[20] It has also been demonstrated that polymer thickness, dielectric constant, and surface energy are important determinants of the

Dr. X. Kong, P. E. Rudnicki, Dr. S. Choudhury, Prof. Z. Bao, Prof. J. Qin
Department of Chemical Engineering
Stanford University
Stanford, CA 94305, USA
E-mail: xiankong@stanford.edu; jianq@stanford.edu

 The ORCID identification number(s) for the author(s) of this article can be found under <https://doi.org/10.1002/adfm.201910138>.

DOI: 10.1002/adfm.201910138

local morphology of Li deposits.^[26] However, a mechanistic understanding of the effects of these factors is missing.

Distinct lithium growth morphologies are experimentally observed, which are highly dependent on operating conditions during lithium deposition. Typical lithium morphologies include mossy deposits and dendritic structures.^[27] While “mossy” structures can lead to electrolyte depletion due to their large reactive surface area, dendritic structures are most dangerous for penetrating the separator and causing cell shorting and safety hazards.^[27,28] Fractal dendrites are known to occur even under conditions in which the classical Sand’s time model predicts that transport limitation should not occur,^[29] and are more prevalent at high current densities that are desirable for practical battery operation.

Previous theoretical or modeling studies of Li deposition are largely based on continuum models. Linear stability analysis^[30] is the most widely used framework to study lithium deposition stability. An analysis conducted in the reaction-limited regime predicted that lithium dendrites can be mechanically suppressed when the shear modulus of the separator is about twice that of lithium.^[9,10] Further analysis within this scheme also predicted a density-driven stability mechanism, in which dendrites can be suppressed due to hydrostatic stresses when the molar volume of Li^+ in the electrolyte is smaller than that of Li metal.^[31] Another linear stability analysis in the mass-transport-limited regime focused on the stabilizing effects of anion immobilization.^[20,32] Linear stability analysis is limited to the nucleation step and cannot model the dynamics of lithium growth. Additionally, linearization of the system requires many simplifying assumptions, and generally only 2D systems are considered. Phase-field models have also been applied to study the development of dendritic growths during lithium deposition.^[33–35] However, this approach may not accurately capture processes away from the dendrite surface,^[36] such as altered ionic transport through a polymer coating.

Compared to the continuum approaches, molecular dynamics (MD) is more straightforward and can capture both deposition dynamics and dendrite morphology. However, because of the discrepancy between dendrite dimensions ($\approx \mu\text{m}$) and molecular size, coarse-graining (CG) is necessary. A 2D coarse-grained model has been developed which confirmed that dendrites are more likely to form with increasing overpotential and showed that pulsed charging can effectively suppress dendrite growth.^[37] The model was later extended to include 2D electromigration,^[38] and was used to study how diffusive dendrite annealing can be promoted to control dendrite growth.^[39,40] A separate 2D model incorporated both the bulk and surface diffusion of Li, as well as deposition kinetics, but neglected electromigration.^[41] No study on the effects of polymer coating has been reported.

In this work, we develop a 3D coarse-grained molecular simulation model to study the deposition of lithium on an electrode in the presence of a polymer coating layer. The polymer coating is modeled as a mesh of interconnected beads. The difference in dielectric permittivity between the polymer layer and the electrolyte is explicitly treated by imposing a spatially varying dielectric profile in the Poisson equation for the electric potential. This coarse-grained model is designed for the transport-limited regime, in which lithium deposition is fast compared

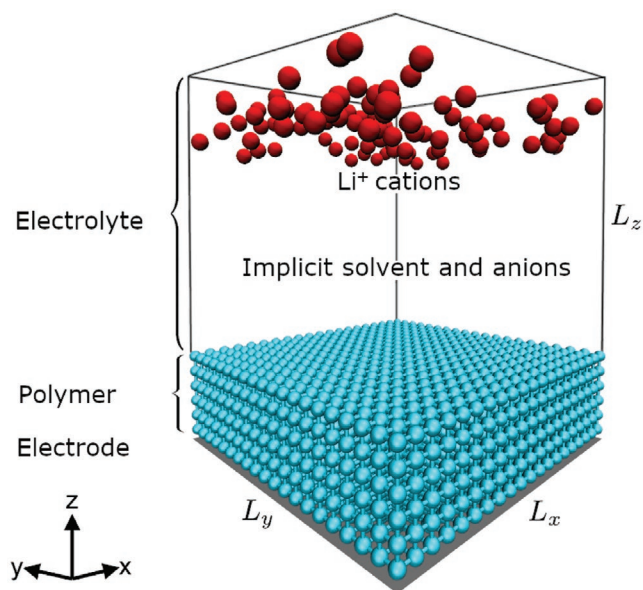


Figure 1. The model schematic and an initial deposition configuration. The box is $20 \times 20 \times 25$ nm, and the lithium cations are distributed randomly at the top of the box ($z = 25$ nm).

to SEI growth and fractal morphology is observed. The growth mechanism of mossy dendrites is highly dependent on the mechanical properties of the SEI and the choice of electrolyte. Resolving those chemical and physical heterogeneities would require atomistic resolutions^[42] that cannot be captured by our model. The details of our model are presented in the next section, which is followed by systematic explorations of the effects of polymer elasticity, relaxation time, dielectric permittivity, and coating thickness on the lithium deposition behavior. Our main findings and perspective on future studies are summarized in the final section.

2. Model and Simulation

Our model simulates the deposition of lithium cations onto a lithium metal anode through an implicit liquid electrolyte and an explicit polymer layer under an applied electric potential, as shown in **Figure 1**. In our model, the current collector is assumed to be planar and its surface coincides with the plane $z = 0$ as well as the lower boundary of the simulation box. The lengths of the box along the x , y , and z directions are L_x , L_y , and L_z . Their values are tabulated in **Table 1**. Periodic boundary conditions are imposed along the x and y directions to reduce the finite size effect. Solvents and anions are modeled implicitly, and a constant medium dielectric permittivity is assigned. The coating polymer is modeled as an interconnected network of mobile beads while the lithium cations are modeled as mobile spheres with one elementary charge e . The deposited lithium beads are modeled as fixed spheres having the same electric potential as the electrode.

The motions of Li^+ and polymer beads are treated as Brownian.^[38] The equation of motion has the standard form $\Delta r = \sqrt{2D\Delta t} \mu + \mu F\Delta t$, where Δr is the displacement of the bead

Table 1. The model parameters and the default values.

Parameter	Symbol	Unit	Value
Box size	L_x, L_y, L_z	nm	20, 20, 25
Time step	Δt	μs	1
Number of Li^+	$n(\text{Li}^+)$	–	100
Polymer layers	–	–	4
Maximum lithium height	H_{max}	nm	15
Reaction distance	d_{cut}	nm	0.6
Cathode voltage	Φ_{cathode}	V	0.5
Anode voltage	Φ_{anode}	V	0
Bond length between polymer beads	b	nm	1
Bond coefficient between polymer beads	k	eV nm^{-2}	10
Exclusion size: polymer beads	$\sigma_{\text{pp}}^{\text{a)}$	nm	1
Exclusion size: polymer and cation beads	$\sigma_{\text{pi}}^{\text{b)}$	nm	0.5
Exclusion size: polymer and metal beads	$\sigma_{\text{pm}}^{\text{c)}$	nm	1.25
Exclusion size: cation beads	σ_{ii}	nm	1.0
Exclusion strength: polymer beads	χ_{pp}	eV nm^{-2}	10
Exclusion strength: polymer and cation beads	χ_{pi}	eV nm^{-2}	10
Exclusion strength: polymer and metal beads	χ_{pm}	eV nm^{-2}	10
Exclusion strength: cation beads	χ_{ii}	eV nm^{-2}	10
Li^+ diffusivity	D_i	$\text{nm}^2 \mu\text{s}^{-1}$	2×10^{-2}
Li^+ mobility	μ_i	$\text{nm}^2 (\text{eV } \mu\text{s})^{-1}$	8×10^{-1}
Polymer diffusivity	D_p	$\text{nm}^2 \mu\text{s}^{-1}$	2.5×10^{-5}
Polymer mobility	μ_p	$\text{nm}^2 (\text{eV } \mu\text{s})^{-1}$	1×10^{-3}
Pressure force	F_{pressure}	eV nm^{-1}	0.1
Polymer dielectric constant	$\epsilon_p/\epsilon_0^{\text{d)}$	–	20
Electrolyte dielectric constant	$\epsilon_{\text{electrolyte}}/\epsilon_0^{\text{d)}$	–	20

^{a)}p refers to polymer; ^{b)}i refers to lithium ion; ^{c)}m refers to metallic lithium; ^{d)}The potential field is determined by the ratio between the polymer permittivity and that of the electrolyte, for given electrolyte permittivity.

during a time period of Δt , and D and μ are diffusivity and mobility, which are related by the Einstein relation $D = k_B T \mu$. Here k_B is the Boltzmann constant and the temperature T is set to a constant (298 K) throughout this work. The first term represents the diffusive motion and μ is a random unit vector. The second term is the driven motion caused by the net force \mathbf{F} exerted on the beads. Since the mobility of polymer beads is much lower than that of lithium ions, the diffusive motion of polymer beads is negligibly small, and the movement of polymers is dominated by the mobility term.

The polymer beads feel forces due to bond connection (V^{bond}), excluded volume interaction ($V^{\text{exclusion}}$), and repulsion from the electrode surface (V^{wall}). To avoid unphysical polymer movement away from the electrode, a constant body pressure force ($\mathbf{F}^{\text{pressure}}$) is applied to each polymer bead. Therefore, the total force acting on polymer beads is given by $\mathbf{F}_i = -\nabla_{\mathbf{r}_i} (V^{\text{bond}} + V^{\text{exclusion}} + V^{\text{wall}}) + \mathbf{F}^{\text{pressure}}$. The bond interaction between polymer beads i, j is harmonic, $V_{ij}^{\text{bond}}(r) = \frac{k}{2}(r - b)^2$, where $r = |\mathbf{r}_i - \mathbf{r}_j|$ is the distance between beads i and j , k is the bond strength, and b is the equilibrium bond length. The

volume exclusion between beads is modeled using a soft pair potential, $V_{ij}^{\text{exclusion}}(r)$, which is given by $\frac{1}{2} \chi_{ij} (r - \sigma_{ij})^2$ if $r \leq \sigma_{ij}$ and 0 otherwise. Here, χ_{ij} is the penalty for size overlap and $\sigma_{ij} = (\sigma_i + \sigma_j)/2$ is the average of the diameters of beads i and j . To prevent the polymer beads from penetrating the current collector, a Steele interaction between the polymer beads and the current collector is imposed:^[43]

$$V^{\text{wall}} = 2\pi\epsilon^2\sigma^2\rho_w \left[\frac{2}{5} \left(\frac{\sigma}{z} \right)^{10} - \left(\frac{\sigma}{z} \right)^4 \right], \text{ where}$$

σ is the size of the polymer bead, ρ_w is the packing density of the collector wall, ϵ is the interaction strength, and z is the distance from the bead to the collector surface.

The cationic beads experience the volume exclusion force and the electrostatic force. The volume exclusion force is treated in the same way as for the polymer beads. The electrostatic force is derived from the electric potential, which is resolved by solving 3D Poisson's equation, $\nabla \cdot \epsilon(\mathbf{r}) \nabla \Phi(\mathbf{r}) = 0$. Here, $\Phi(\mathbf{r})$ and $\epsilon(\mathbf{r})$ are the electric potential and the dielectric permittivity at position \mathbf{r} . As bulk charge separation is highly unfavorable even at short length scales, we assume that the ambipolar diffusion condition holds, that is, all the charged particles are neutralized by particles of opposite charge.^[44] Therefore, charge neutrality is assumed everywhere when Poisson's equation is solved.^[45] A finite difference relaxation is used to solve Poisson's equation,^[46] and the grid size is set to 0.5 nm.

An important feature of polymer-protected deposition is that the deposition rate and quality are affected by the discrepancy between the dielectric permittivities of the polymer and the bulk electrolyte.^[47] This effect is included in our model by introducing a spatially varying dielectric permittivity in Poisson's equation: the permittivity is set to that of polymers in the polymer-rich domain, and that of the electrolytes otherwise.

The top boundary of the simulation box (Figure 1) is assumed to be the cathode and is assigned a fixed electric potential Φ_{cathode} , while the anode current collector and the deposited lithium beads are assigned a fixed electric potential Φ_{anode} . We used a higher voltage difference (0.5 V) for polymer coated conditions, in contrast to 0.1 V for the bare electrode cases. This is analogous to applying a higher overpotential to achieve galvanostatic conditions in a more resistive system.

The distribution of the electric potential is affected by the morphology of the deposited lithium (Figure 2a) and the dielectric screening due to the polymer coating (Figure 2b). Near the tip of the dendrite, the electric potential varies more rapidly, as seen in the closely spaced potential contour lines near dendrite tips in Figure 2a, implying a stronger electric field. This

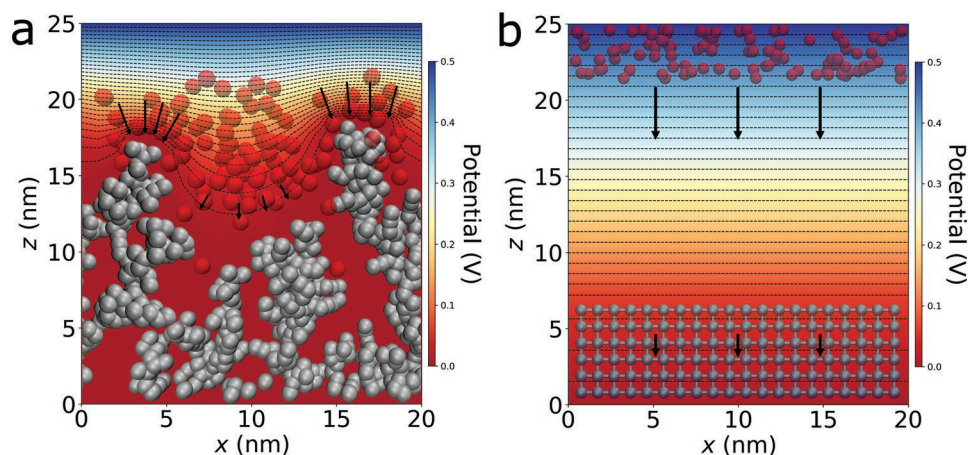


Figure 2. Lithium morphology and polymer dielectric permittivity strongly affect the electric potential field. Arrows schematically represent electric field strength. The current collector is located at $z = 0$ nm. a) Electric potential field near a bare dendrite structure. The dendrite is equipotential with the current collector. The potential contours correspond to a 2D slice of the full potential field. b) Electric potential field in the presence of a polymer-coated flat electrode. The dielectric constant of the polymer is larger than that of the electrolyte for this case, causing the electric field to be diminished within the polymer.

effect causes the lithium ions to aggregate to the tip through motion directed by electrostatic forces. In the presence of polymer coating with higher dielectric permittivity than the electrolyte, Figure 2b shows that the field strength weakens within the polymer due to stronger dielectric screening, that is, reduction of field strength due to polymer polarization. This demonstrates that our model captures the influence of dielectric inhomogeneity. This screening effect is determined by the ratio between the permittivities of the polymer and the electrolyte. Experimentally, this ratio can range from values much less than 1 for nonpolar polymer coatings to 2–3 or even greater for fluorinated polymers in typical electrolytes such as 1,3-dioxolane/dimethoxyethane (DOL/DME) or diethyl carbonate (DEC).^[26,48,49]

The simulation of lithium deposition proceeds as follows. Prior to ion deposition, all the lithium ions are placed at the top of the simulation box (Figure 1). We have tested that the initial placement of lithium ions does not significantly affect the deposition results (Figure S1, Supporting Information), since the initially placed ions only account for a small fraction of the total number of ions deposited. Then, a bias electric potential along the z direction is turned on, which causes the cations to migrate toward the anode. Once a Li^+ cation comes into contact with the collector surface ($z_{\text{Li}}^+ < d_{\text{cut}}/2$) or the previously deposited metallic Li ($r_{\text{Li}}^+, \text{Li} < d_{\text{cut}}$), it becomes a metallic Li bead and remains fixed for the remainder of the simulation. After the formation of a metallic Li, a new Li^+ is released from the top of the simulation box at random (x, y) positions to keep the number of Li^+ constant. When the deposited lithium beads reach a preset height (H_{max}), which was set constant throughout all simulations, the simulation is halted. Table 1 lists the default values of the parameters used in most simulations. The alternative values used for studying the effects of individual parameters will be explicitly specified. To simplify symbol usage, we express all the interaction energies in units of eV.

Several approximations are necessary in order to analyze the diffusive and migratory behaviors of lithium ions with

reasonable computational costs. The ionic diffusion coefficient is scaled down, following the approach of Aryanfar *et al.*^[38] The diffusion coefficient of lithium cations is on the order of $10^2 \text{ nm}^2 \mu\text{s}^{-1}$ in both carbonate and ether electrolytes.^[50,51] Hence, our ionic diffusion coefficient ($2 \times 10^{-2} \text{ nm}^2 \mu\text{s}^{-1}$) in the implicit solvent is three to four orders of magnitude lower than experimental values. The thickness of the coating layer in our model ($\approx \text{nm}$) is also scaled down relative to the experimental values ($\approx \mu\text{m}$). The number of the lithium ions deposited per cycle and the total deposition time are also scaled down such that the effects of the dielectric screening and polymer coating thickness match the experimental observations. The radius of the lithium cation beads is chosen as 0.3 nm, larger than physical lithium ions, whose van der Waals radius is 0.18 nm.^[52] Therefore, lithium beads are meant to represent not only a single lithium ion. It is a highly coarse-grained representation, so that only the qualitative trend is captured with tolerable computational cost. As previously stated, our study examines the effects of the polymer coating on Li deposition in the transport-limited regime, in which dangerous dendritic deposits are formed. Since it is believed that Li deposition is faster than SEI growth in this regime,^[42] SEI effects are neglected in this study. Similarly, the polymer degradation at the surface and side reactions are neglected.

3. Results and Discussion

The simulation results obtained from our coarse-grained model reveal that the morphology of the deposited lithium is affected by the stiffness, the characteristic relaxation time, the dielectric permittivity, and the thickness of the polymer coating. For favorable combinations of coating properties, dendritic growth may be suppressed. To identify the optimal condition, the effects of each factor are investigated. The results are presented below, after an overview of the various deposition scenarios.

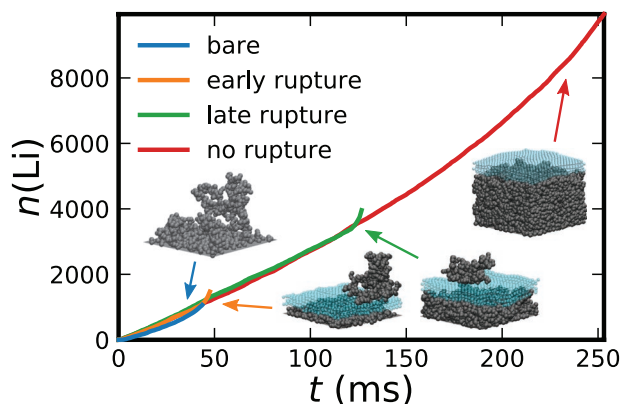


Figure 3. Deposition profiles under representative coating conditions. Note that the presence of a polymer coating decreases the current. Therefore, a lower electrode potential (analogous to the applied overpotential) is used for the bare case (0.1 V) than the coated cases (0.5 V) to achieve a similar current.

The deposition dynamics is conveniently quantified by the number of deposited lithium ions over time. Higher terminal deposition number implies a denser deposited morphology. Four representative deposition curves simulated under comparable charging current are shown in **Figure 3**, which includes the deposition on the bare electrode and on electrodes coated with three distinct polymer layers with different properties (details in Table S1, Supporting Information). In all these cases, the number of deposited lithium beads increases steadily with time. The blue curve, for the bare electrode, terminates slightly before 50 ms, when the top of the dendrite reaches the cutoff height. Without a coating, the lithium morphology quickly becomes dendritic due to preferential cationic motion toward randomly nucleated tips. The coated electrodes generally result in a higher number of deposited lithium beads, but the detailed dynamics depends on the choice of coating properties. For the orange and the green curves, initially the deposition is uniform; however, at times 50 and 125 ms respectively, a randomly formed sharp tip ruptures the polymer layer. Following the rupture, the polymer coating acts as a barrier to deposition in areas away from the tip. The exposed lithium tip becomes a hot spot for further deposition, and an avalanche deposition ensues. For the case represented by the red curve, no such film rupture occurs, and a continuous and uniform deposition persists. This suggests that an ideal coating should remain intact and uniform during deposition, damping or even completely suppressing the inherent instability caused by aggregation of ions at randomly occurring tips due to the localized strong electric field (Figure 2).

The following sections examine systematically how the physical properties of a polymer coating modulate the deposition dynamics. Although the use of a coarse-grained model prevents quantitative prediction, the trends drawn from systematic parametric screening are expected to be valuable guides to experiment.

3.1. Polymer Stiffness

During deposition, randomly occurring lithium tips with high curvature are expected to impose a large strain on the polymer

coating. This may lead to rupture if the polymer is not mechanically resilient. We studied the influence of polymer stiffness by varying the bond strength between polymer beads k , which is proportional to the bulk modulus of the polymer. The deposition curves for a range of bond strengths are summarized in **Figure 4a**.

The deposition profiles in **Figure 4a** are nearly congruent prior to film rupture, implying negligible impact of the stiffness on the deposition rate. However, as shown in **Figure 4b**, the deposition morphology is susceptible to the choice of bond strength. When the bond strength is either too low or too high, the number of deposited lithium is reduced, corresponding to a more porous structure and dendritic morphology. For lower bond strength, a growing lithium tip can easily punch through the polymer, leading to dendrite growth. The rupture point occurs relatively soon after deposition starts. In the final deposited morphology, multiple dendrites grow through the polymer coating, creating a “forest-like” structure (**Figure 4b** inset and **Figure 4c** liquid-like case). The mechanically weak polymer is unable to suppress or delay randomly occurring dendritic instabilities (see Movie S1, Supporting Information). The limiting case of low k is representative of the behavior of liquid electrolytes, where no bonds are present and therefore $k = 0$. In this extreme condition, no benefit is obtained from the coating.

On the other hand, if the bond strength is too high, the polymer coating cannot adapt to changes in the morphology of the deposited lithium. As shown in Movie S2, Supporting Information, during deposition, the polymer coating moves slowly like a planar rigid body with the growing lithium structure. The stiff polymer coating acts as a rigid, porous membrane, and lithium is deposited in the membrane pores. In rigid polymers, static microporosity can be observed due to imperfect, frustrated packing of stiff chain backbones, with a more dynamic microporosity seen in polymers with faster segmental motion.^[53] These pores can enhance ionic conductivity but are also potential growth pathways for dendrites. Once the deposited lithium penetrates the polymer layer and reaches the bulk electrolyte, explosive growth results in the “mushroom-like” morphology (**Figure 4b** inset and **Figure 4c** solid-like case). An analogous failure mechanism has been observed in porous, cross-linked polymer coatings with pore sizes above a critical radius.^[54,55]

Uniform deposition occurs at an intermediate range of k values. Within this range, the polymer coating can adapt to the evolving lithium growth front, directing cations away from randomly occurring tips by condensing its local structure. It is also strong enough to prevent growing dendrites from breaking through (see Movie S3, Supporting Information; **Figure 4b** inset and **Figure 4c** viscoelastic case). This is analogous to “solid-liquid” interfacial layers which mechanically resist dendrite growth on short timescales but flow and adapt to changing lithium fronts on longer timescales.^[56] Typical mechanical responses of polymers to growing lithium tips are further illustrated in **Figure S2**, Supporting Information.

3.2. Polymer Relaxation Time

Lithium deposition is heterogeneous, stochastic, and involves dramatic structural evolution such as dendritic growth. The

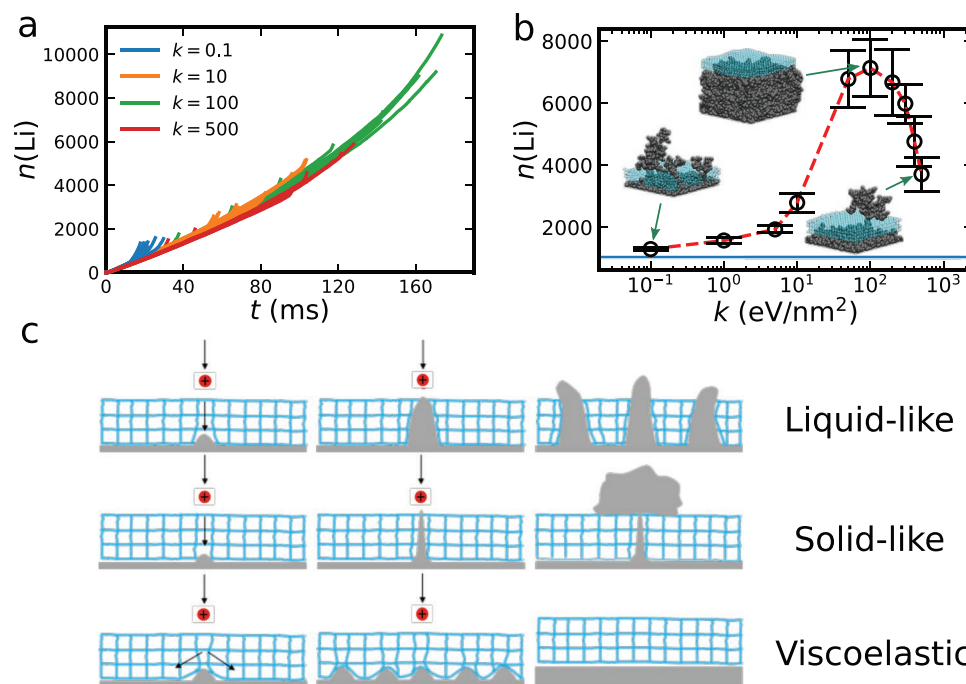


Figure 4. Lithium deposition number is maximized at intermediate bond strengths, while deposition rate is constant relative to bond strength. a) The number of deposited lithium beads as a function of simulation time, showing the influence of bond strength (k) on lithium deposition. Multiple deposition profiles with different random number seeds are shown for each bond strength value. b) The final number of deposited lithium beads versus bond strength between polymer beads. Error bars represent standard errors. The blue horizontal line is the number of deposited lithium beads on a bare collector at a voltage of 0.1 V. The inset images are final deposition morphologies at the indicated conditions. c) Schematic of the effect of polymer mechanical properties on the growth and morphology of nucleated dendrites.

dendritic growth may further penetrate and rupture protective coating layers.^[57] Being adaptive and able to dynamically conform to an evolving growth front is critical to the suppression of dendritic growths. To quantify such adaptability, one may consider the relaxation time $\tau \sim \eta/G$ where η is the viscosity and G the modulus.^[58] Within our model, the modulus is proportional to the bond strength k , and the viscosity is reciprocal to the mobility μ of polymer beads. The previous section has shown that the stiffness k greatly influences the ability of the polymer layer to adapt. An analogous screening of the effects of viscosity η , shown in Figure S3, Supporting Information, indicates that higher polymer bead mobility often enhances the coating quality. More exhaustive screening, as discussed below, reveals that bead mobility and chain stiffness cooperate to dictate film adaptability.

To quantify the film adaptability, we consider the intrinsic relaxation time of the polymer coating. It can be defined as the relaxation time for the fluctuation of the film height profile, and is calculated by fitting the initial decay in the autocorrelation function of the average height to an exponential (Figure S4, Supporting Information). The relaxation time is obtained by conducting simulations in the absence of lithium deposition (the lifetime of height fluctuation is longer for more liquid-like coating). By varying the bond strength k and the bead mobility μ over four orders of magnitude, the relaxation times were varied from 0.01 to 100 ms (Figure 5a). As expected, the relaxation time monotonically decreases with increasing bead mobility or increasing bond strength. Moreover, re-scaling the relaxation time by μ and k (which gives the dimensionless value $\tau\mu k$) collapses all times onto a master curve (Figure 5b).

The terminal deposition number for this array of coating layers reveals an optimal parametric window, in a narrow range of τ around 50 to 500 μ s (Figure 5c; Figure S5, Supporting Information). Severely decreased performance occurs at both lower and higher relaxation times, in agreement with the peaked behavior seen in Figure 4b. The mobility and bond strength jointly dictate the polymer performance. Once the bond strength is higher than a minimum threshold ($k > 1$ eV nm⁻²), the number of deposited lithium increases in a narrow range of relaxation times (Figure S5, Supporting Information), which means that the effect of the coating can be captured by a single parameter, the relaxation time. This is related to the experimental measurement of the terminal relaxation time in linear rheological measurements. Previous studies have shown improved deposition with the “solid-liquid” polymer layers, which performed better than chemically similar liquid-like and solid-like coatings.^[56] In a study of multiple polymer coatings, the viscoelastic polymer layers outperformed the elastomers and the rigid, semi-crystalline polymers.^[26] However, no systematic experimental study has been done to accurately examine the role of polymer coating mechanics in suppressing deposition instabilities. Our work reveals a clear connection between polymer viscoelasticity and deposition morphology and stability. As discussed in the previous section, viscoelastic polymers are both mechanically robust on short timescales and adaptable on longer timescales, creating an ideal combination of flexibility and strength for an artificial layer. This non-monotonic relationship between morphological stability and the mechanical

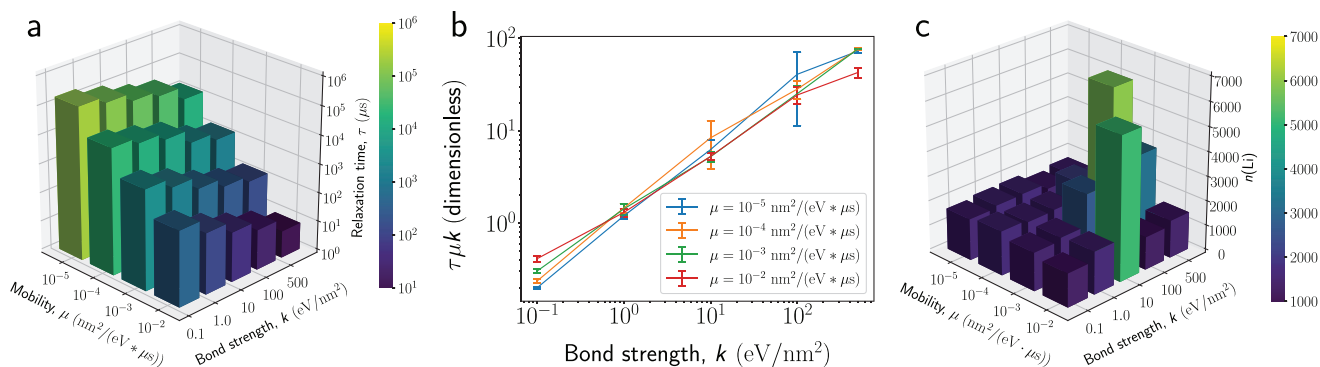


Figure 5. Polymer relaxation time alters deposition stability. a) Relaxation time for polymer height fluctuations monotonically changes as a function of bond strength and polymer bead mobility. b) Non-dimensionalized relaxation times collapse onto a master plot. c) The number of deposited lithium is optimized within a narrow range of relaxation times.

strength of a polymer coating is a clear departure from the conventional understanding.

3.3. Polymer Dielectric Permittivity

A randomly formed lithium tip that ruptures the polymer coating grows due to the exaggerated deposition near the tip after its appearance. The local aggregation is mainly driven by the strong electric field near the tip, whose strength depends on the dielectric response of the polymer layer. Therefore, increasing the dielectric permittivity may slow down the directed motion of lithium ions near the lithium tips, and consequently reduce the chance of coating rupture. This is indeed supported by the simulated deposition dynamics and the deposition numbers shown in **Figure 6**. We note that this investigation is possible only when Poisson's equation with a spatially varying dielectric permittivity.

The results in **Figure 6b** demonstrate that the number of the deposited lithium beads increases steadily with the increased dielectric permittivity of the polymer layer, consistent with the expectation that the higher permittivity screens the electric potential more effectively and hence damps the directed drift motion of lithium ions toward a lithium tip. Nevertheless, the stronger dielectric screening also suppresses the drift

motion of lithium cations along the z direction, and reduces the deposition flux, which is clearly seen from the decreased slope in the deposition curves for polymers with higher dielectric permittivity (**Figure 6a**). Therefore, we conclude that higher polymer dielectric permittivity favors uniform deposition at the cost of low effective current. Experimentally, polymer coatings with polar functional groups have been shown to improve the quality of lithium deposition relative to the non-polar polymers,^[59,60] and the high-polarity β phase PVDF coatings outperformed the low-polarity α phase.^[47] It is important to note that while previously, a high polymer dielectric permittivity has been linked to an increased exchange current density and therefore a decreased reaction overpotential,^[26] this is a kinetic effect at the lithium–polymer interface. Our model, on the other hand, reveals an increased transport overpotential at high dielectric constant.

3.4. Coating Thickness

Polymer thickness is a tunable design parameter. Experimentally, due to the roughness of the electrode surface and the statistical character of the coating process, a coating with a minimum thickness is required to ensure that the current collector is fully covered, leaving no bare surface as a hot spot

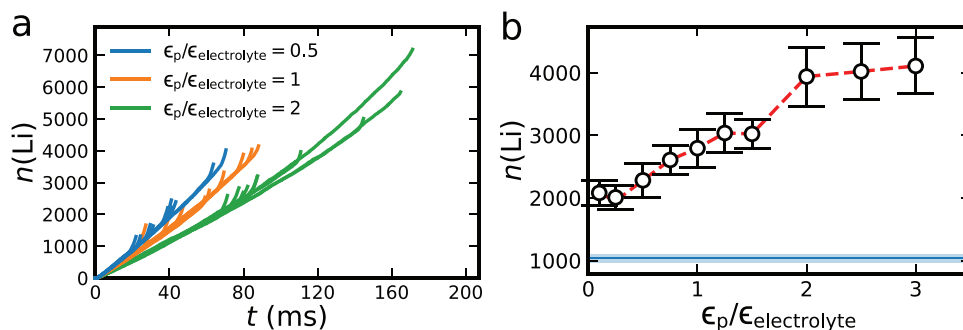


Figure 6. Deposition number increases with the polymer permittivity, but deposition rate decreases. a) The number of deposited lithium beads as a function of simulation time, showing the influence of the ratio between polymer and electrolyte dielectric constant ($\epsilon_p/\epsilon_{\text{electrolyte}}$) on lithium deposition. Multiple deposition profiles with different random number seeds are shown for each polymer dielectric constant. b) The final number of deposited lithium beads versus $\epsilon_p/\epsilon_{\text{electrolyte}}$. Error bars represent the standard errors. The blue horizontal line is the number of deposited lithium beads on a bare collector at a voltage of 0.1 V.

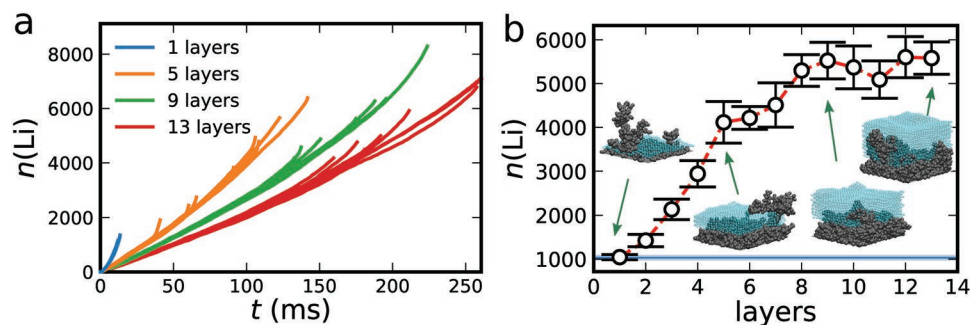


Figure 7. Deposition number increases with coating thickness, but deposition rate decreases. a) The number of deposited lithium beads as a function of simulation time showing the influence of coating thickness (number of polymer layers) on lithium deposition. Multiple deposition profiles with different random number seeds are shown for each coating thickness. b) The final number of deposited lithium beads versus number of polymer layers. Error bars represent the standard errors. The blue horizontal line is the number of deposited lithium beads on a bare collector at a voltage of 0.1 V.

for dendrite growth. Additionally, optimal thicknesses have been experimentally observed, indicating that the benefits of a polymer coating are maximized for uniform but relatively thin coatings.^[26,61] To provide a mechanistic view of the thickness effect, we investigated the deposition dynamics by varying the number of polymer layers.

The deposition profiles, shown in **Figure 7**, verify that thicker polymer coatings slow down the ion motion, reduce the deposition rate and, therefore, lower the effective current. When the coating is thin (one or two layers in our model), no significant improvement is obtained over the bare case, although the collector is fully covered. The simulation trajectories demonstrate that, since the polymer coating is thin, almost any random occurring dendrite tip can punch through it. Although this mirrors the experimental finding that a minimum thickness is needed to improve the deposition quality,^[26] the mechanisms are different because experimentally a minimum coating thickness is required for the complete coverage of a spin-coated current collector. However, the enhancement of deposition morphology tends to saturate with thickness, as shown in the nearly plateauing regime when the number of layers exceeds about nine (**Figure 7b**). We therefore propose that, in practice, an optimal coating thickness should be employed,^[26] which effectively suppresses the dendrite growth without significantly decreasing the deposition current.

4. Summary

A coarse-grained 3D molecular model which explicitly accounts for the dielectric heterogeneity is developed and is employed to investigate the mechanism of lithium dendrite growth suppression with a polymer coating. The deposition dynamics is simulated for a range of molecular parameters, including the stiffness, the relaxation time, the dielectric permittivity, and the coating thickness. The results suggest that the film stiffness and the bead mobility should be optimized simultaneously to achieve the desired relaxation time leading to the uniform lithium deposition (**Figure 5**). Outside this optimal regime, a faster relaxation will lead to facile lithium penetration and a “forest-like” dendrite structure, while a slower relaxation will lead to poor adaptability and allow the deposited lithium to grow through the pores in the polymer coating, giving rise to

the “mushroom-like” dendrite structure. Increasing the dielectric permittivity of the polymer coating improves the deposition quality by damping the directed motion of lithium ions toward the growing tip. A minimum thickness of the polymer coating is required to effectively suppress dendrites, while an intermediate thickness should be chosen in order to maintain a sufficiently high charging rate.

These phenomenological results leave clear room for further studies. As noted above, certain aspects of the predictions have been observed in experiments, including the improved performance by viscoelastic coating layers,^[25,26,56] the improved deposition with polar, high-permittivity coating layers,^[47,59,60] and the existence of an optimal coating thickness.^[26,61] Additional experiments that systematically explore the viscoelastic response of polymer coatings would help unveil the relative importance of the various effects revealed by our analyses. The model can be generalized in several ways: 1) The current implementation treats the polymer layer as a permanent network; implementing dynamic bonds would allow for studies of dynamic polymer coatings. 2) The roughness of the electrode can be explicitly introduced to investigate the deposition more realistically. 3) Since mossy growth is a major concern, it would be important to extend the model to the reaction-limited regime. 4) SEI effects and polymer reactivity are additional important concerns. Our coarse-grained model could, in theory, be used to investigate the effect of an inorganic SEI. However, lithium transport in the SEI usually occurs in atomic-scale pathways through crystalline structures or along grain boundaries and lithium desolvation at the interface must be considered. Incorporating these effects in our model with atomistic details calculated *ab initio* is necessary for studying the effects of an inorganic SEI.^[62] Finally, it would be important to analyze the instability inherent in the continuum transport process, and evaluate the simulation results within such a framework. The fundamental understanding accumulated through these modeling efforts will provide the basis for engineering the optimal polymer coating layer for stable lithium deposition.

Supporting Information

Supporting Information is available from the Wiley Online Library or from the author.

Acknowledgements

X.K. and P.E.R. contributed equally to this work. J.Q. acknowledges the 3M Non-Tenured Faculty Award and the Hellman Scholar Award. This research was supported by the Assistant Secretary for Energy Efficiency and Renewable Energy, Office of Vehicle Technologies of the U. S. Department of Energy through the Advanced Battery Materials Research (BMR) Program (Battery500 Consortium). This material is based upon work supported by the (P.E.R.) under Grant No. DGE-1656518. The authors thank Jeffrey Lopez and Chibueze Amanchukwu for fruitful discussions and feedback.

Conflict of Interest

The authors declare no conflict of interest.

Keywords

lithium dendrites, lithium metal batteries, molecular simulations, polymer coating

Received: December 4, 2019

Revised: January 21, 2020

Published online: February 17, 2020

- [1] X.-B. Cheng, R. Zhang, C.-Z. Zhao, Q. Zhang, *Chem. Rev.* **2017**, *117*, 10403.
- [2] P. Albertus, S. Babinec, S. Litzelman, A. Newman, *Nat. Energy* **2018**, *3*, 16.
- [3] D. Lin, Y. Liu, Y. Cui, *Nat. Nanotechnol.* **2017**, *12*, 194.
- [4] W. Xu, J. Wang, F. Ding, X. Chen, E. Nasybulin, Y. Zhang, J.-G. Zhang, *Energy Environ. Sci.* **2014**, *7*, 513.
- [5] J. Zhao, L. Liao, F. Shi, T. Lei, G. Chen, A. Pei, J. Sun, K. Yan, G. Zhou, J. Xie, C. Liu, Y. Li, Z. Liang, Z. Bao, Y. Cui, *J. Am. Chem. Soc.* **2017**, *139*, 11550.
- [6] S. Choudhury, C. T.-C. Wan, W. I. Al Sadat, Z. Tu, S. Lau, M. J. Zachman, L. F. Kourkoutis, L. A. Archer, *Sci. Adv.* **2017**, *3*, 4.
- [7] G. Zheng, S. W. Lee, Z. Liang, H.-W. Lee, K. Yan, H. Yao, H. Wang, W. Li, S. Chu, Y. Cui, *Nat. Nanotechnol.* **2014**, *9*, 618.
- [8] M. S. Kim, J.-H. Ryu, Deepika, Y. R. Lim, I. W. Nah, K.-R. Lee, L. A. Archer, W. Il Cho, *Nat. Energy* **2018**, *3*, 889.
- [9] C. Monroe, J. Newman, *J. Electrochem. Soc.* **2004**, *151*, A880.
- [10] C. Monroe, J. Newman, *J. Electrochem. Soc.* **2005**, *152*, A396.
- [11] B. Commarieu, A. Paoletta, J.-C. Daigle, K. Zaghbi, *Curr. Opin. Electrochem.* **2018**, *9*, 56.
- [12] G. M. Stone, S. A. Mullin, A. A. Teran, D. T. Hallinan, A. M. Minor, A. Hexemer, N. P. Balsara, *J. Electrochem. Soc.* **2012**, *159*, A222.
- [13] J. Janek, W. G. Zeier, *Nat. Energy* **2016**, *1*, 16141.
- [14] M. Chintapalli, T. N. P. Le, N. R. Venkatesan, N. G. Mackay, A. A. Rojas, J. L. Thelen, X. C. Chen, D. Devaux, N. P. Balsara, *Macromolecules* **2016**, *49*, 1770.
- [15] I. Villaluenga, S. Inceoglu, X. Jiang, X. C. Chen, M. Chintapalli, D. R. Wang, D. Devaux, N. P. Balsara, *Macromolecules* **2017**, *50*, 1998.
- [16] W. Zhou, S. Wang, Y. Li, S. Xin, A. Manthiram, J. B. Goodenough, *J. Am. Chem. Soc.* **2016**, *138*, 9385.
- [17] M. D. Tikekar, S. Choudhury, Z. Tu, L. A. Archer, *Nat. Energy* **2016**, *1*, 16114.
- [18] Q.-C. Liu, J.-J. Xu, S. Yuan, Z.-W. Chang, D. Xu, Y.-B. Yin, L. Li, H.-X. Zhong, Y.-S. Jiang, J.-M. Yan, X.-B. Zhang, *Adv. Mater.* **2015**, *27*, 5241.
- [19] K. Liu, P. Bai, M. Z. Bazant, C.-A. Wang, J. Li, *J. Mater. Chem. A* **2017**, *5*, 4300.
- [20] M. D. Tikekar, L. A. Archer, D. L. Koch, *Sci. Adv.* **2016**, *2*, 7.
- [21] L. Li, L. Ma, B. A. Helms, *Macromolecules* **2018**, *51*, 7666.
- [22] Q. Pan, D. M. Smith, H. Qi, S. Wang, C. Y. Li, *Adv. Mater.* **2015**, *27*, 5995.
- [23] S. Choudhury, R. Mangal, A. Agrawal, L. A. Archer, *Nat. Commun.* **2015**, *6*, 10101.
- [24] Y. Liu, D. Lin, P. Y. Yuen, K. Liu, J. Xie, R. Dauskardt, Y. Cui, *Adv. Mater.* **2017**, *29*, 1605531.
- [25] G. Zheng, C. Wang, A. Pei, J. Lopez, F. Shi, Z. Chen, A. D. Sendek, H.-W. Lee, Z. Lu, H. Schneider, M. M. Safont-Sempere, S. Chu, Z. Bao, Y. Cui, *ACS Energy Lett.* **2016**, *1*, 1247.
- [26] J. Lopez, A. Pei, J. Y. Oh, G.-J. N. Wang, Y. Cui, Z. Bao, *J. Am. Chem. Soc.* **2018**, *140*, 11735.
- [27] P. Bai, J. Li, F. R. Brushett, M. Z. Bazant, *Energy Environ. Sci.* **2016**, *9*, 3221.
- [28] Q. Cheng, L. Wei, Z. Liu, N. Ni, Z. Sang, B. Zhu, W. Xu, M. Chen, Y. Miao, L.-Q. Chen, W. Min, Y. Yang, *Nat. Commun.* **2018**, *9*, 2942.
- [29] K. N. Wood, M. Noked, N. P. Dasgupta, *ACS Energy Lett.* **2017**, *2*, 664.
- [30] W. Mullins, R. Sekerka, *J. Appl. Phys.* **1964**, *35*, 444.
- [31] Z. Ahmad, V. Viswanathan, *Phys. Rev. Lett.* **2017**, *119*, 056003.
- [32] M. D. Tikekar, L. A. Archer, D. L. Koch, *J. Electrochem. Soc.* **2014**, *161*, A847.
- [33] D. R. Ely, A. Jana, R. E. Garcia, *J. Power Sources* **2014**, *272*, 581.
- [34] R. A. Enrique, S. DeWitt, K. Thornton, *MRS Commun.* **2017**, *7*, 658.
- [35] Z. Hong, V. Viswanathan, *ACS Energy Lett.* **2018**, *3*, 1737.
- [36] J. Tan, A. M. Tartakovsky, K. Ferris, E. M. Ryan, *J. Electrochem. Soc.* **2016**, *163*, A318.
- [37] M. Z. Mayers, J. W. Kaminski, T. F. Miller III, *J. Phys. Chem. C* **2012**, *116*, 26214.
- [38] A. Aryanfar, D. Brooks, B. V. Merinov, W. A. Goddard, A. J. Colussi, M. R. Hoffmann, *J. Phys. Chem. Lett.* **2014**, *5*, 1721.
- [39] A. Aryanfar, D. J. Brooks, A. J. Colussi, B. V. Merinov, W. A. Goddard III, M. R. Hoffmann, *Phys. Chem. Chem. Phys.* **2015**, *17*, 8000.
- [40] A. Aryanfar, T. Cheng, A. J. Colussi, B. V. Merinov, W. A. Goddard III, M. R. Hoffmann, *J. Chem. Phys.* **2015**, *143*, 134701.
- [41] F. Hao, A. Verma, P. P. Mukherjee, *ACS Appl. Mater. Interfaces* **2018**, *10*, 26320.
- [42] P. Bai, J. Guo, M. Wang, A. Kushima, L. Su, J. Li, F. R. Brushett, M. Z. Bazant, *Joule* **2018**, *2*, 2434.
- [43] J. Stecki, *Langmuir* **1997**, *13*, 597.
- [44] Q. Cheng, L. Wei, Z. Liu, N. Ni, Z. Sang, B. Zhu, W. Xu, M. Chen, Y. Miao, L.-Q. Chen, W. Min, Y. Yang, *Nat. Commun.* **2018**, *9*, 2942.
- [45] M. Z. Bazant, *Phys. Rev. E* **1995**, *52*, 1903.
- [46] W. H. Press, S. A. Teukolsky, W. T. Vetterling, B. P. Flannery, *Numerical Recipes 3rd Edition: The Art of Scientific Computing*, 3rd ed., Cambridge University Press, New York **2007**.
- [47] J. Luo, C.-C. Fang, N.-L. Wu, *Adv. Energy Mater.* **2018**, *8*, 1701482.
- [48] V. Tiwari, G. Srivastava, *J. Polym. Res.* **2014**, *21*, 587.
- [49] N. N. Rajput, V. Murugesan, Y. Shin, K. S. Han, K. C. Lau, J. Chen, J. Liu, L. A. Curtiss, K. T. Mueller, K. A. Persson, *Chem. Mater.* **2017**, *29*, 3375.
- [50] K. Hayamizu, Y. Aihara, S. Arai, C. G. Martinez, *J. Phys. Chem. B* **1999**, *103*, 519.
- [51] K. Hayamizu, *J. Chem. Eng. Data* **2012**, *57*, 2012.
- [52] A. Bondi, *J. Phys. Chem.* **1964**, *68*, 441.
- [53] C. Li, S. M. Meckler, Z. P. Smith, J. E. Bachman, L. Maserati, J. R. Long, B. A. Helms, *Adv. Mater.* **2018**, *30*, 1704953.
- [54] Z. Tu, M. J. Zachman, S. Choudhury, S. Wei, L. Ma, Y. Yang, L. F. Kourkoutis, L. A. Archer, *Adv. Energy Mater.* **2017**, *7*, 1602367.

- [55] B. Zhu, Y. Jin, X. Hu, Q. Zheng, S. Zhang, Q. Wang, J. Zhu, *Adv. Mater.* **2017**, *29*, 1603755.
- [56] K. Liu, A. Pei, H. R. Lee, B. Kong, N. Liu, D. Lin, Y. Liu, C. Liu, P.-c. Hsu, Z. Bao, Y. Cui, *J. Am. Chem. Soc.* **2017**, *139*, 4815.
- [57] D. Lin, Y. Liu, W. Chen, G. Zhou, K. Liu, B. Dunn, Y. Cui, *Nano Lett.* **2017**, *17*, 3731.
- [58] P. C. Hiemenz, T. P. Lodge, *Polymer Chemistry*, CRC Press, Boca Raton, FL **2007**.
- [59] Z. Liang, G. Zheng, C. Liu, N. Liu, W. Li, K. Yan, H. Yao, P.-C. Hsu, S. Chu, Y. Cui, *Nano Lett.* **2015**, *15*, 2910.
- [60] C. Chi-Hao, C. Sheng-Heng, M. Arumugam, *Adv. Sustainable Syst.* **2017**, *1*, 1600034.
- [61] Y. Gao, Y. Zhao, Y. C. Li, Q. Huang, T. E. Mallouk, D. Wang, *J. Am. Chem. Soc.* **2017**, *139*, 15288.
- [62] Y. Chen, C. Ouyang, L. Song, Z. Sun, *J. Phys. Chem.* **2011**, *115*, 7044.